Pediatric RESEARCH

www.nature.com/pr

BASIC SCIENCE ARTICLE

Characterization of the innate immune response in a novel murine model mimicking bronchopulmonary dysplasia

Chanèle Cyr-Depauw[1,2], Maria Hurskainen[1,2], Arul Vadivel[1,2], Ivana Mižíková[1,2], Flore Lesage[1,2] and Bernard Thébaud[1,2,3]

BACKGROUND: Bronchopulmonary dysplasia (BPD), the most common complication of prematurity, arises from various factors that compromise lung development, including oxygen and inflammation. Hyperoxia has been used to mimic the disease in newborn rodents. The use of a second hit to induce systemic inflammation has been suggested as an added strategy to better mimic the inflammatory aspect of BPD. Here we report a novel 2 hit (2HIT) BPD model with in-depth characterization of the innate immune response, enabling mechanistic studies of therapies with an immunomodulatory component.

METHODS: C57BL/6N mice were exposed to 85% O_2 from postnatal day (P)1 to P7, and received postnatally (P3) *Escherichia coli* LPS. At various timepoints, immune activation in the lung and at the systemic level was analyzed by fluorescence-activated cell sorting (FACS), and gene and protein expressions.

RESULTS: 2HIT mice showed fewer alveoli, increased lung compliance, and right ventricular hypertrophy. A transient proinflammatory cytokine response was observed locally and systemically. Type 2 anti-inflammatory cytokine expression was decreased in the lung together with the number of mature alveolar macrophages. Simultaneously, a Siglec-F intermediate macrophage population emerged.

CONCLUSION: This study provides long-term analysis of the 2HIT model, suggesting impairment of type 2 cytokine environment and altered alveolar macrophage profile in the lung.

Pediatric Research (2021) 89:803–813; https://doi.org/10.1038/s41390-020-0967-6

IMPACT:

- We have developed a novel 2HIT mouse BPD model with postnatal LPS and hyperoxia exposure, which enables mechanistic studies of potential therapeutic strategies with an immunomodulatory component.
- This is the first report of in-depth characterization of the lung injury and recovery describing the evolution of the innate immune response in a standardized mouse model for experimental BPD with postnatal LPS and hyperoxia exposure.
- The 2HIT model has the potential to help understand the link between inflammation and impaired lung development, and will enable testing of new therapies in a short and more robust manner.

INTRODUCTION

Bronchopulmonary dysplasia (BPD) is the most common chronic lung disorder of infancy. Among neonatal morbidities, BPD has the highest cost in initial neonatal intensive care unit stay.[1] BPD was first described nearly 50 years ago by Northway et al.[2] as a chronic respiratory disease that developed in preterm newborns exposed to mechanical ventilation and oxygen supplementation. With improved survival, infants at risk of developing BPD are now born at earlier gestational ages (23–26 weeks). The hallmarks of the lung pathology are being described as arrested lung development, including fewer and larger alveoli with less septation, thickening of alveolar septa, and impaired development of capillary network.[3] These changes may lead to life-long respiratory morbidity, including asthma, reduced exercise capacity, early-onset emphysema, and pulmonary hypertension (PH).[4]

Studies of disease mechanism in BPD have been restricted to animal models, due to limited access to patient lung samples. The most common models include the exposure of term rodents to hyperoxia of varying concentration (40–100%) and length (3 days–4 weeks).[5,6] Bonikos et al.[7] were the first to report that exposure of mice to hyperoxia results in chronic lung injury characterized by alveolar simplification reminiscent of BPD. Subsequently, many groups have studied in more detail the physiological and molecular effects of hyperoxia on newborn rodent lungs. Hyperoxia induces innate immune response by stimulating the secretion of several cytokines and chemokines, and subsequent recruitment of neutrophils, monocytes, and macrophages to the lungs.[8] Recent evidence suggest that during normal mouse lung development, the first breath induces differentiation of alveolar macrophages into mature M2 (anti-inflammatory)

[1]Sinclair Centre for Regenerative Medicine, Ottawa Hospital Research Institute, Ottawa, ON, Canada; [2]Department of Cellular and Molecular Medicine, University of Ottawa, Ottawa, ON, Canada and [3]Children's Hospital of Eastern Ontario Research Institute, Ottawa, ON, Canada
Correspondence: Bernard Thébaud (bthebaud@ohri.ca)
These authors contributed equally: Chanèle Cyr-Depauw, Maria Hurskainen

Received: 4 September 2019 Revised: 21 April 2020 Accepted: 26 April 2020
Published online: 20 May 2020

macrophages.[9,10] Conversely, neonatal hyperoxic exposure induces a proinflammatory M1 phenotype in the alveolar macrophages.[11,12] However, the inflammatory injury in rodent hyperoxia models is only moderate.[13] Considering that perinatal inflammation and episodes of sepsis,[14] as well as pneumonia,[15] are important risk factors for the development of BPD, the use of a second hit to induce systemic inflammation has been suggested and described as an improved strategy to mimic the pathogenesis of clinical BPD.[16–18]

Translation of potentially life-saving therapies into the clinic is unacceptably slow. It has been argued that one of the underlying reasons is the lack of methodological rigor in the development of preclinical animal models.[19] Here, we present the 2HIT model, where the mice receive two independent hits, including 85% hyperoxia from P1 to P7 and low-dose systemic *Escherichia coli* LPS at P3 to mimic perinatal inflammation in premature newborn infants at risk of developing BPD. We hypothesized that the 2HIT model would provide a short, robust, and standardized mouse model for experimental BPD with impaired innate immunity, which would allow both understanding disease pathogenesis, with a focus on inflammation and testing of new therapies, and establishing mode of action. We demonstrate the evolution of the inflammatory response over the course of both the injury and repair phases during the first month of life. Furthermore, we show that the number of anti-inflammatory homeostatic alveolar macrophages decreases significantly after injury, accompanied by a simultaneous increase in a Siglec-F intermediate population of lung macrophages. Our findings suggest that the 2HIT model causes both local and systemic type 1 cytokine responses, and, importantly, disturbs the homeostatic type 2 cytokine environment of the lung during the crucial stages of lung development, which may in turn contribute to the altered lung architecture. To our knowledge, this is the first report of in-depth characterization of the lung injury and recovery describing the evolution of the innate immune response in a 2HIT mouse model with postnatal LPS and hyperoxia exposure.

MATERIALS AND METHODS

Animals

All procedures were approved by the Animal Care Committee of the University of Ottawa and animal care was performed in accordance with institutional guidelines. Pregnant C57BL/6N mice were delivered on embryonic days (E)15–E17 from Charles Rivers, Saint Constant, QC, Canada. Pups from all litters were randomized at P1 (P0 is the day of birth) and allocated to one dam to obtain a litter size of six to seven pups per dam. The number of pups in each litter was maintained to an equal number (±1) by euthanizing control pups when deceased pups were found in 2HIT litters. Two experimental hits were used in this study: hyperoxia (85% O_2) from P1 until P7 (sealed plexiglass chambers with continuous oxygen monitoring [BioSpherix, Redfield, NY]) and intraperitoneal (i.p.) injection of 1 mg/kg LPS (*E. coli* O55:B5, Sigma-Aldrich L2880, St. Louis, MO) at P3 (Fig. 1a). Hyperoxic dams were exchanged with normoxic dams every 48 h to avoid oxygen toxicity. The experimental groups were as follows: (1) hyperoxia and LPS (2HIT), (2) room air (RA) control, (3) RA and LPS (RA + LPS), and (4) hyperoxia (O_2). Animals were sacrificed by i.p. injection of pentobarbital sodium (Euthanyl, 0.2 mL, 65 mg/mL).

Histology

Lungs were harvested for histology as described earlier at P8, P15, 4 weeks, and 3 months.[20] Spleen, liver, and kidney samples (P15, 4 weeks, and 3 months) were collected from both RA and 2HIT animals and fixed for 48 h in 10% formalin at room temperature (RT). After fixation, all organs were embedded in paraffin, sectioned at 4 µm, and stained with hematoxylin and eosin (H&E) by the University of Ottawa, Louise Pelletier Histology Core Facility. Alveolar size was quantified by a motorized microscope stage, using the mean linear intercept (MLI) estimation.[21]

Lung function testing

At 4 weeks and 3 months timepoints, a tracheostomy was performed and lung function (pressure volume [PV] loop) was assessed using flexiVent (SCIREQ, Montreal, QC, Canada) as described earlier.[20] Average of three measurements per mouse was used.

Flow cytometry

Lung or spleen cells were stained with lung immune cell or with spleen macrophage antibodies, respectively (Supplemental Table S1a [online]). In addition, P2–P5 lungs were stained with lung macrophage M1/M2 panel and P8–4 week lungs with the lung immune cell panel with M1/M2 markers. After staining, samples were fixed with 4% paraformaldehyde (PFA). Fluorescence minus one (FMO), single, and no stain controls were used as necessary. Flow cytometry was performed by Ottawa Hospital Research Institute core facility using BD LSRFortessa (Beckton Dickinson Biosciences, Franklin Lakes, NJ). Sample compensation was performed with BD FACSDIVA software and data were analyzed using FlowJo v10 (FlowJo LLC, Ashland, OR).

Quantitative RT-PCR

Complementary DNA (cDNA) was reverse transcribed from 1 µg of total RNA using iScript™ Reverse Transcription Supermix (Bio-Rad cat#1708841). Quantitative RT-PCR (qRT-PCR) analysis was performed using CFX96 or CFX384 Touch Real-Time PCR (Bio-Rad). Reactions were performed in 20 µL volume using 1.2 nM primer concentration, 10 µL iQ™ SYBR Green Supermix (Bio-Rad, cat#1708882) and 5 µL of diluted cDNA (1:5 in ddH_2O). Primer sequences are described in Supplementary Table S1b (online). The qRT-PCR program consisted of 95 °C for 3 min, followed by 40 cycles of denaturation at 95 °C (15 s), annealing at 57 °C (for 30 s), and extension at 72 °C (30 s). Melting curves were obtained by increasing temperature by 0.5 °C every 5 s from 65 °C to 95 °C after the last extension phase to validate primer specificity. Optimal annealing temperature was determined by testing a range of eight different temperatures between 54 °C and 66 °C. Efficiency was calculated using the formula $10^{(-1/\text{slope of standardization})} - 1$. The normalized expression level of the target genes for each condition was calculated using the average threshold cycle (Ct) value from triplicate measurements by the Pfaffl method.[22] *Hprt* was identified as a stable housekeeping gene using geNorm and BestKeeper.

Multiplex assay

Lung tissue homogenates were diluted to equal amount of protein (8690 µg/mL) and serum was collected from whole blood samples (cardiac puncture), and then diluted 1:2 with phosphate-buffered saline. Cytokines/chemokines were quantified simultaneously by Eve Technologies Corp., Calgary, AB, Canada using a Discovery Assay (Mouse Cytokine Array/Chemokine Array 31-Plex [Lung P3, P8, and P15 and Serum P2, P3, P5, and P8] or Mouse High Sensitivity T Cell Discovery Array 18-plex [Lung P29]) (Supplementary Table S2 [online]). The minimum detectable concentration starts at 0.3 pg/mL.

Statistics

Statistical analyses were performed using GraphPad Prism version 7.0c (GraphPad Software, Inc., La Jolla, CA). Outliers were identified using Grubbs' test and normal distribution using Shapiro–Wilk normality test. *P* values ($P < 0.05$ was considered significant) were obtained with *t* test (unpaired, two-tailed) or log-rank (Mantel–Cox) test for Kaplan–Meier curves or one-way ANOVA with Tukey's multiple comparison post hoc testing to compare results between four groups. Data are represented as the mean with standard deviation (SD).

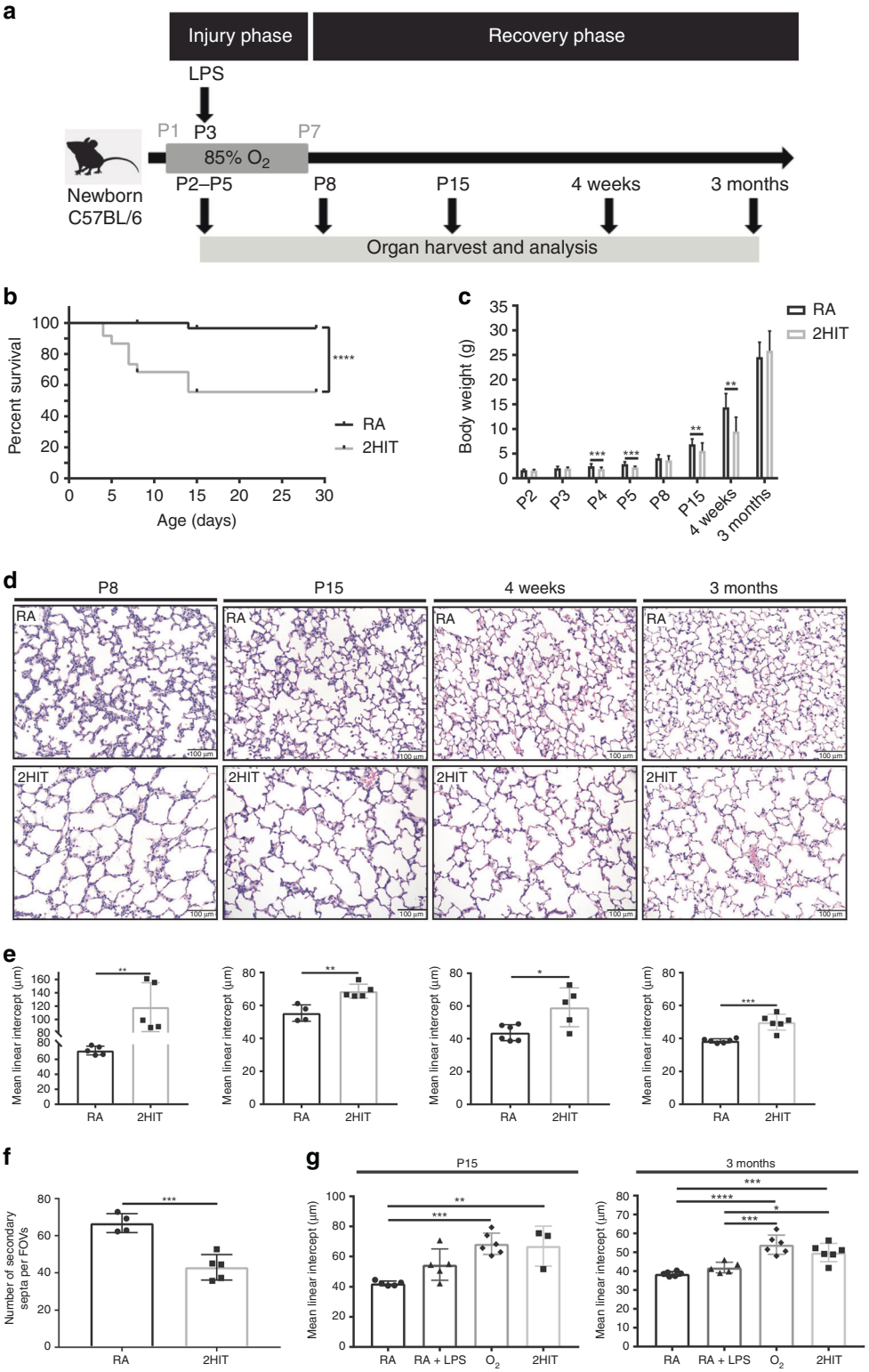

Fig. 1 Survival, body weight, and morphometric analysis of RA, RA + LPS, O_2, and 2HIT lungs. a Experimental design and timelines. **b** Kaplan–Meier survival curve ($n = 73$ [RA] and $n = 60$ [2HIT]). **c** Body weight gain in RA animals compared to 2HIT animals (P2, P4, and P5, $n = 12$ [RA and 2HIT]; P3, $n = 38$ [RA], $n = 43$ [2HIT]; P8, $n = 14$ [RA], $n = 11$ [2HIT]; P15, $n = 22$ [RA], $n = 15$ [2HIT], 4 weeks, $n = 18$ [RA], $n = 13$ [2HIT]; 3 months, $n = 6$ [RA and 2HIT]). **d** Representative images of H&E-stained lung sections of RA and 2HIT animals at P8, P15, 4 weeks, and 3 months. **e** Quantification of alveolar size using the MLI method in RA and 2HIT lung tissue sections at P8, P15, 4 weeks, and 3 months ($n = 4$–6/group). **f** Quantification of secondary septa at P15 ($n = 4$ [RA] and $n = 5$ [2HIT]). **g** Quantification of alveolar size using the MLI method in RA, RA + LPS, O_2, and 2HIT lung tissue sections at P15 and 3 months ($n = 5$–6/group, except for 2HIT group at P15, where $n = 3$). Individual data points shown for each bar graph represent individual mice from multiple litters. Values are represented as the mean ± SD. P value < 0.05 was considered significant. Significant results are shown as $^*P \le 0.05$, $^{**}P \le 0.01$, $^{***}P \le 0.001$, and $^{****}P \le 0.0001$.

RESULTS

2HIT model causes increase in mortality and decrease in body weight of experimental animals

Exposure of mouse pups to hyperoxia and LPS (2HIT) induced a significant increase in mortality compared to pups kept in normoxia (RA) (Fig. 1b). In addition, 2HIT animals had a significantly lower body weight from P4 until 4 weeks of age as compared to RA animals (Fig. 1c). No significant body weight differences were observed at 3 months. To compare the extent of mortality and reduction in body weight in the 2HIT model with single hits (O_2, 85% or LPS), the survival and body weight were assessed at P15 and 3 months. Survival of 2HIT animals was decreased compared to RA + LPS and O_2 animals, but this was not significant (Supplementary Fig. S1a [online]). At P15, RA + LPS, O_2, and 2HIT animals had a significantly lower body weight compared to RA animals, but no significant difference between all injury groups was observed (Supplementary Fig. S1b [online]). However, *t* test analysis did show significant decreased in body weight of 2HIT animals compared to RA + LPS animals. No significant difference in body weight was observed between all groups at 3 months of age.

2HIT animals show altered lung structure and function, as well as right ventricular hypertrophy

Lungs of 2HIT animals had larger and fewer alveoli at P8, P15, 4 weeks, and 3 months (Fig. 1d). Moreover, lungs of 2HIT animals had a significantly higher MLI compared to the lungs of RA animals at all timepoints, indicating that the alveoli were larger in size (Fig. 1e). The number of secondary septa in the 2HIT group was significantly decreased compared to the RA group at P15 (Fig. 1f). To compare the extent of lung injury in the 2HIT model with single hits (O_2, 85% or LPS), the MLI was studied at P15, and 3 months. No significant difference in MLI was observed in the 2HIT group compared to the O_2 group. MLI of the O_2 group was significantly increased compared to the RA group. No significant increase in MLI was observed in the RA + LPS group compared to the RA group. However, MLI of O_2 and 2HIT groups were significantly higher compared to the RA + LPS group at 3 months, but not at P15. (Fig. 1g).

Lung function showed that the 2HIT model induced an upward shift of the PV loop and a significant increase in volume at 30 cmH_2O compared to the RA group at 4 weeks and 3 months suggesting increased lung compliance (Fig. 2a, b). Salazar–Knowles equation parameters were extracted from the PV loop. Static compliance (Cst) was significantly increased in the 2HIT group at 4 weeks and 3 months compared to the RA group, as well as inspiratory capacity (*A*) (Fig. 2c, d). Hysteresis (area under the PV loop) in the 2HIT group, representative of the work of breathing, was also significantly increased compared to the RA group at 4 weeks and 3 months (Fig. 2e).

To compare 2HIT long-term lung function with single hits (O_2, 85% or LPS), the PV loop was studied at 3 months. The PV loop of O_2 and 2HIT animals was shifted upwards. Significant increase in volume at 30 cmH_2O was observed in O_2 animals when compared to RA, RA + LPS, and 2HIT animals, and in 2HIT animals when compared to RA animals (Fig. 2f, g).

Finally, we observed right ventricular hypertrophy (RVH) in 2HIT animals, but not in single hit animals, compared to RA animals at 3 months of age, as measured by the Fulton's index (Fig. 2h).

2HIT model does not induce long-term pulmonary fibrotic changes

Lung fibrosis was assessed by quantifying hydroxyproline content by colorimetry and by collagen staining using the Masson's trichrome in 3-month-old animals. No difference in hydroxyproline content was observed between RA and 2HIT animals (Supplementary Fig. S1c [online]). Moreover, no visible increase in the amount of parenchymal collagen was observed in 2HIT animals (Supplementary Fig. S1d [online]).

2HIT model activates a local pulmonary and systemic type 1 cytokine response

At the messenger RNA (mRNA) level, gene expression levels of *Il1b* and *Tnfa* were significantly increased 3 h after LPS injection at P3 (Fig. 3a, b). While *Il1b* was found to be one of the earliest proinflammatory markers during the injury phase (increased by P3), its expression in 2HIT animals had rapidly decreased in the recovery phase at P8 and P14, when it was even lower than in lungs of RA animals. The expression levels of *Il6*, *Tgfb1*, and *Tnfa* showed a second peak in the 2HIT group at the beginning of the recovery phase at P8, and dropped to comparable levels as in the RA group by P14.

At the protein level, we observed a significant increase of several proinflammatory cytokines and chemokines in lung tissue consistent with the gene expression levels. The cytokines interleukin-17 (IL-17), IL-1α, IL-1β, IL-3, tumor necrosis factor-α (TNFα), and IL-6 were highly upregulated in 2HIT animals during the early injury phase at P3 3 h after LPS injection. However, at the beginning of the recovery phase by P8, these cytokine levels had significantly dropped, with only IL-17 and IL-6, together with IL-2, IL-7, interferon-γ (IFNγ), and IL-1α remaining higher than control levels. All chemokines included in the panel were highly upregulated in the injury phase at P3, but not any longer in the beginning of the repair phase at P8, except for macrophage colony-stimulating factor (M-CSF) and granulocyte CSF (G-CSF) (Fig. 4a). Increase in lung chemokine expression was accompanied by recruitment of innate immune cells (macrophages, neutrophils, and monocytes) to the site of inflammation, the lung (Fig. 4b). By the age of 4 weeks, no difference in the level of expression was found between the 2HIT and the RA group for any studied cytokines, chemokines, or immune cells.

In addition to the local pulmonary immune response, we observed a fast transient systemic proinflammatory response. Already early during the injury phase at P2, a significant increase in eotaxin could be detected in the serum of 2HIT when compared to RA animals (Fig. 4c). At P3, only 3 h after the administration of LPS, a peak in proinflammatory cytokine/chemokine expression was observed. The most highly expressed cytokines in the serum were IL-6 and TNFα, followed by the chemokines monocyte chemoattractant protein-1 (MCP-1), macrophage-inflammatory protein 2 (MIP-2), MIP-1α, G-CSF, and MIP-1β. At P5, the cytokine/chemokine levels dropped significantly as compared to P2, with only MCP-1, G-CSF, and MIP-1β remaining higher than the control. In the beginning of the repair phase at P8, we observed no significant differences between cytokine or chemokine levels between the RA and the 2HIT groups, except for a minor increase in MIG (monokine induced by IFN-γ) and IP-10 (IFN-γ-inducible protein-10), and a decrease in keratinocyte-derived chemokine (KC) and interferon-γ (IFNγ).

Overall, we show that the 2HIT model exhibits a fast pulmonary and systemic proinflammatory response, without signs of chronic inflammation.

2HIT model shows decreased pulmonary type 2 cytokine expression

In the lungs of 2HIT animals, we observed a transient decrease in the mRNA expression levels of type 2 cytokine genes *Il4*, *Il10*, and *Il13* both during the injury and beginning of the recovery phases at P3 and P8 (Fig. 5a, b). Also, the expression of M2 macrophage marker *Arg1* was transiently decreased in the beginning of the recovery phase at P8. At the protein level, we observed slightly increased protein levels of IL-4, and IL-5 at P3 and IL-10 and leukemia inhibitory factor (LIF) at both P3 and P8 (Fig. 5c).

In addition, we observed an early transient systemic anti-inflammatory cytokine response in the serum with a peak just after injection with LPS, with increased levels of IL-5, LIF, IL-13, IL-15, and IL-10 and the growth factor VEGF (vascular endothelial growth factor) for a short period of time at P3 (Fig. 5d). The

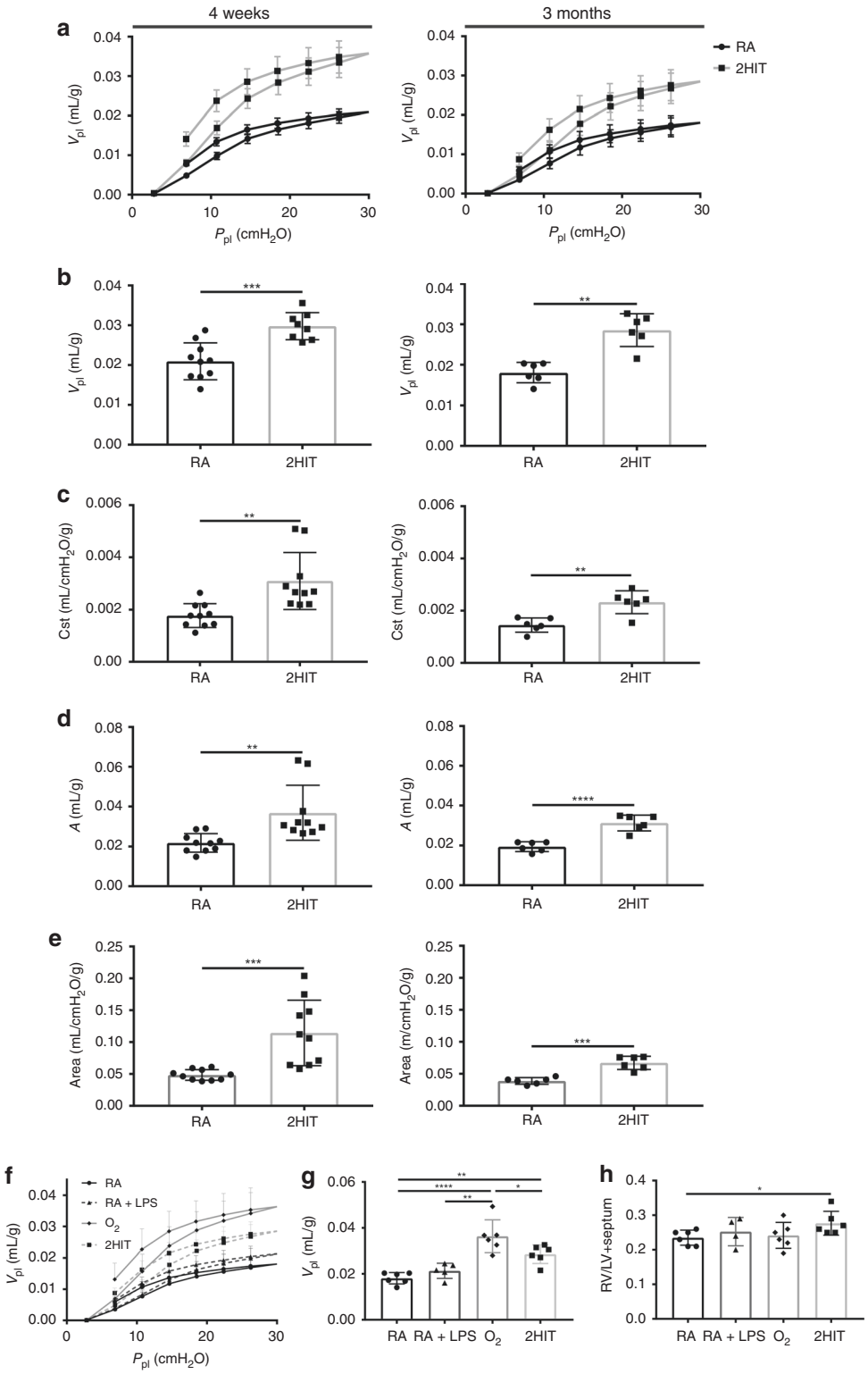

Fig. 2 The effect of LPS, O_2, and 2HIT injuries on lung function and right ventricular hypertrophy. a Body weight-adjusted PV curves for RA and 2HIT animals at 4 weeks and 3 months of age and **b** body weight-adjusted lung volume at peak Ppl 30. **c** Body weight-adjusted static compliance (Cst), **d** body weight-adjusted inspiratory capacity (*A*) and **e** body weight-adjusted hysteresis (area under PV loop) of RA and 2HIT animals at 4 weeks and 3 months of age. **f** Body weight-adjusted PV curves for RA, RA + LPS, O_2, and 2HIT animals at 3 months of age and **g** body weight-adjusted lung volume at peak Ppl 30. **h** Fulton's index quantifying right ventricular hypertrophy of RA, RA + LPS, O_2, and 2HIT animals at 3 months of age. PV curves are shown as the mean volume of all animals within one group at each pressure point. Individual data points shown for each bar graph represent individual mice from multiple litters. Values are represented as the mean ± SD ($n = 4$–10/group). *P* value < 0.05 was considered significant. Significant results are shown as $^*P \le 0.05$, $^{**}P \le 0.01$, $^{***}P \le 0.001$, and $^{****}P \le 0.0001$.

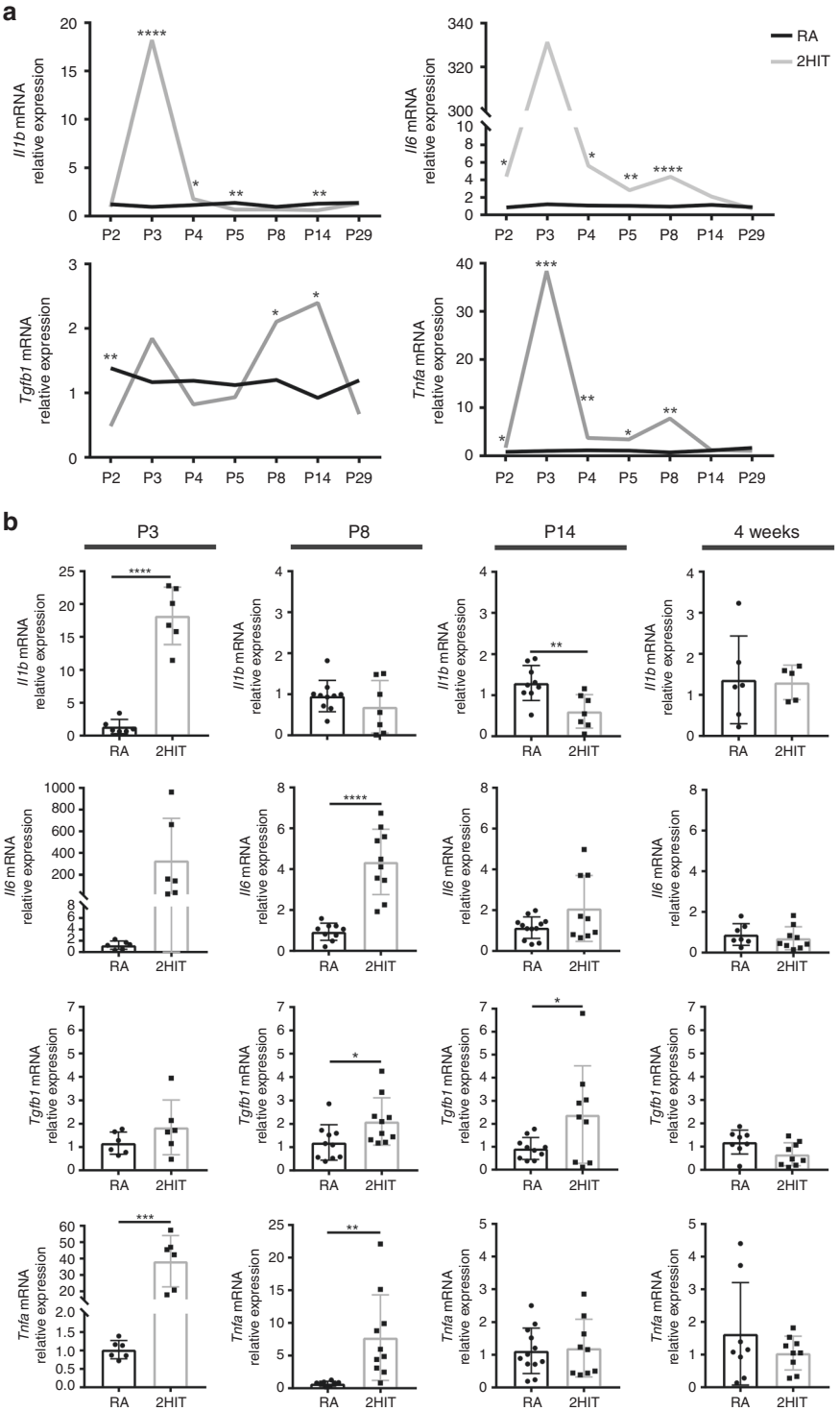

Fig. 3 mRNA expression level of type 1 proinflammatory cytokines in the lung of RA and 2HIT animals. Relative mRNA expression of proinflammatory cytokines *Il1b*, *Il6*, *Tgfb1*, and *Tnfa* in 2HIT animals as compared to RA animals at P2, P3 (3 h after LPS injection), P4, P5, P8, P14, and 4 weeks as **a** a timeline, and **b** individually. Individual data points shown for each bar graph represent individual mice from multiple litters. Values are the means ± SD of two to three independent experiments ($n = 4$–12/group). P value < 0.05 was considered significant. Significant results are shown as $^{*}P \le 0.05$, $^{**}P \le 0.01$, $^{***}P \le 0.001$, and $^{****}P \le 0.0001$.

systemic type 2 cytokine response was no longer detected at P5 (Fig. 5d). Interestingly, the gene expression levels of *Il4* and *Il10* in the lung tissue were simultaneously downregulated, indicating that detected proteins were derived from the circulation and not from the lung resident or recruited cells (Fig. 5b). In conclusion, the results indicate that lung resident and recruited cells do not produce increased quantities of type 2 cytokines after injury in the 2HIT model.

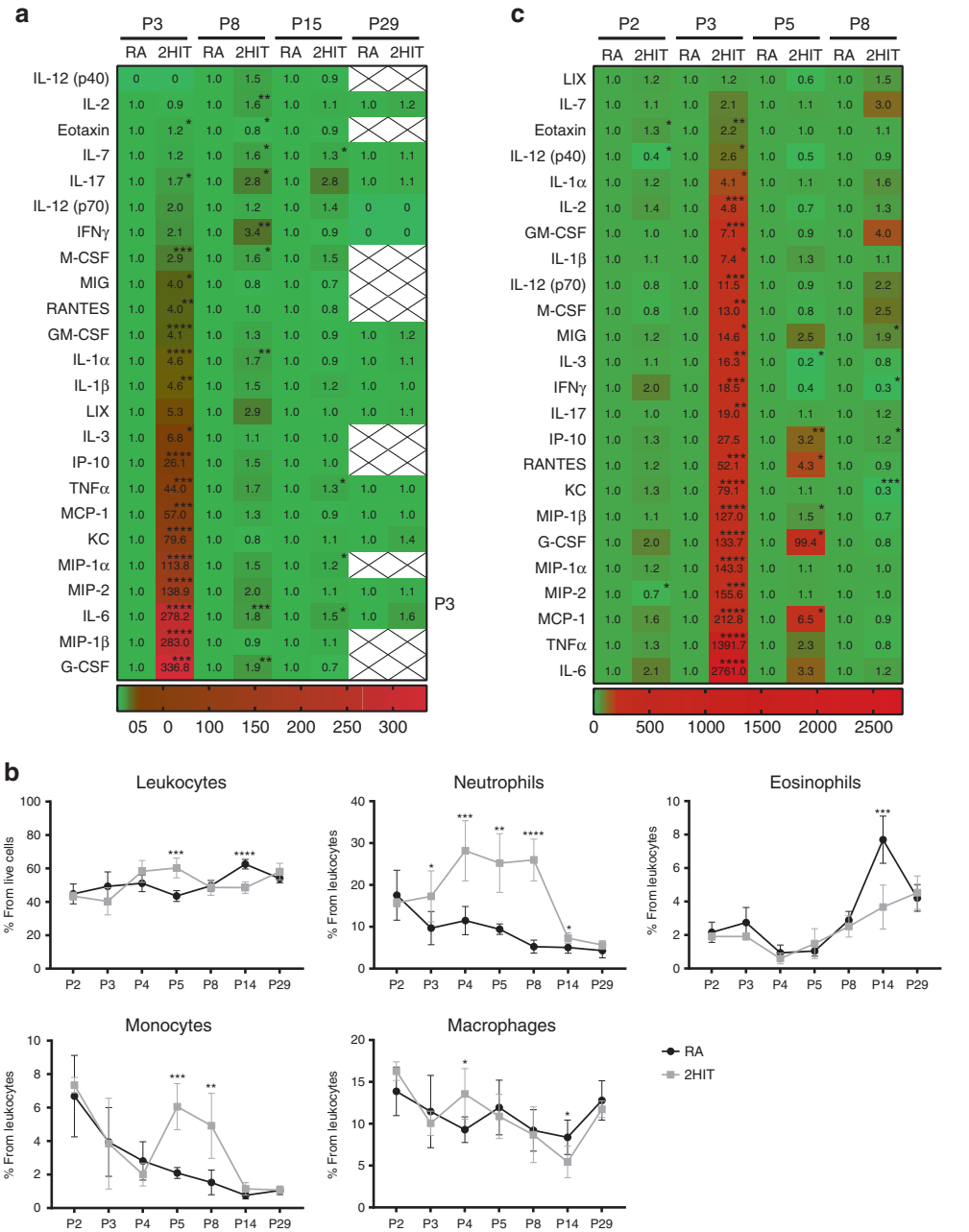

Fig. 4 Innate immune cell counts and proinflammatory cytokine and chemokine protein expression of RA and 2HIT animals. a The protein expression pattern of proinflammatory cytokines and chemokines in the lung (P3 [3 h after LPS injection], $n = 4$ [RA and 2HIT]; P8, $n =$ 4–8 [RA and 2HIT]; P15, $n = 6$ [RA] and $n = 5$–6 [2HIT]; P29, $n = 5$ [RA and 2HIT]). **b** Relative quantities of innate immune cells in the lungs detected by FACS ($n = 4$–6/group). Immune cell populations were analyzed by FACS from dissociated lungs. **c** The protein expression pattern of proinflammatory cytokines and chemokines in the serum (P2, P3 [3 h after LPS injection] and P5, $n = 3$ [RA and 2HIT]; P8, $n = 5$ [RA and 2HIT]). Values for multiplex panel are given as fold change (see Supplementary Table S2 [online] for details). Values are represented as the means ± SD. P value < 0.05 was considered significant. Significant results are shown as $^{*}P \le 0.05$, $^{**}P \le 0.01$, $^{***}P \le 0.001$, and $^{****}P \le 0.0001$.

The number of mature anti-inflammatory lung resident alveolar macrophages decreases in response to the 2HIT injuries

A FACS gating strategy modified from Misharin et al.[23] was used to distinguish between the alveolar (Siglec-F^{high}) and interstitial macrophages (Siglec-F^{-}) as a time course between P8 and 4 weeks timepoints (Supplementary Fig. S2a [online]). We noticed a dramatic reduction in the number of alveolar macrophages in 2HIT animals from P8 onwards (Fig. 6a). This was accompanied by the rise of a Siglec-F^{low} macrophage population (Supplementary Fig. S2b [online]). In contrast, the only significant change—an increase—in the number of interstitial macrophages was observed at P14 (Fig. 6a).

In concordance with the presence of type 1 cytokines such as IFNγ, we observed macrophage polarization towards proinflammatory M1 phenotype in 2HIT animals early during the injury phase. Alveolar macrophages were analyzed using gating strategies described in Supplementary Fig. S2a, c (online), and were found to upregulate the expression of CD86, a commonly used M1 marker, between P3 and P8 (Supplementary Fig. S3a [online] and Fig. 6a). At P8 (beginning of the recovery phase), we

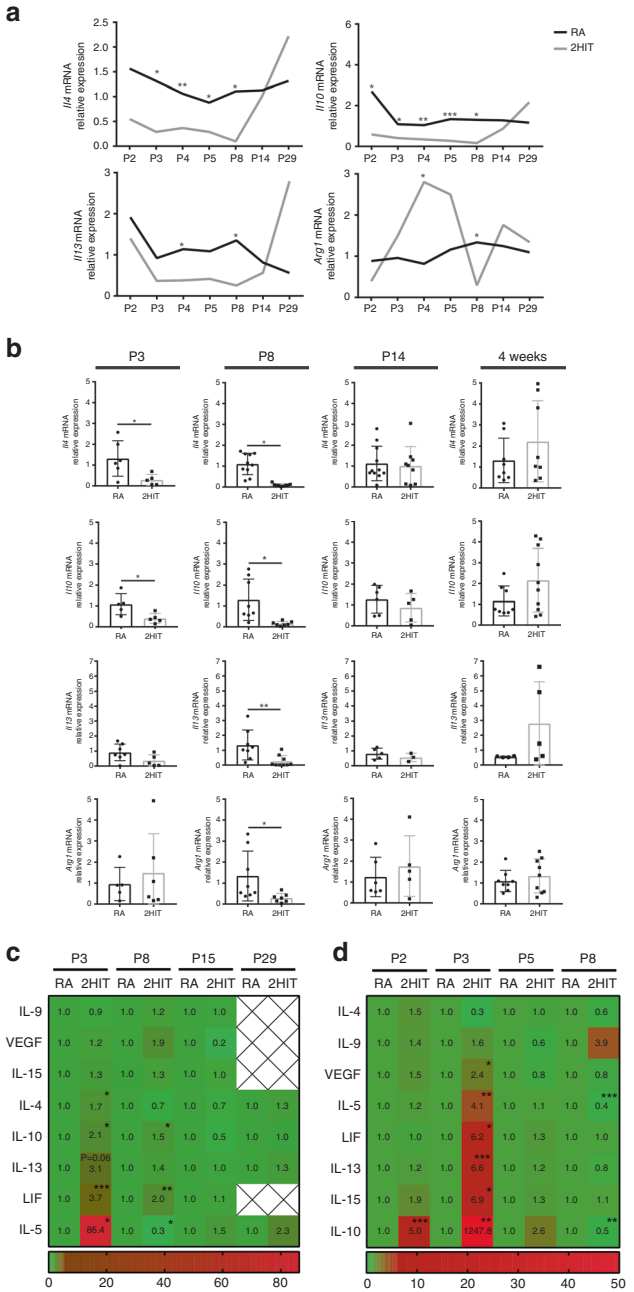

Fig. 5 mRNA expression level of type 2 anti-inflammatory cytokines and arginase-1 in the lung of RA and 2HIT animals, and protein expression level of anti-inflammatory cytokines and chemokines of RA and 2HIT animals. Relative mRNA expression of anti-inflammatory cytokines *Il4*, *Il10*, *Il13*, and *Arg1* in 2HIT animals as compared to RA animals at P2, P3 (3 h after LPS injection), P4, P5, P8, P14, and 4 weeks as **a** a timeline, and **b** individually. Values are the means ± SD of two to three independent experiments ($n = 3$–11/group). **c** The expression pattern of anti-inflammatory cytokines and chemokines in the lung (P3 [3 h after LPS injection], $n = 4$ [RA and 2HIT]; P8, $n = 6$–8 [RA and 2HIT]; P15, $n = 6$ [RA and 2HIT]; P29, $n = 6$ [RA] and $n = 5$ [2HIT]) and **d** in the serum (P2, P3 [3 h after LPS injection] and P5, $n = 3$ [RA and 2HIT]; P8, $n = 5$ [RA and 2HIT]). Values for multiplex panel are given as fold change (see Supplementary Table S2 for details [online]). Individual data points shown for each bar graph represent individual mice from multiple litters. *P* value < 0.05 was considered significant. Significant results are shown as $*P \le 0.05$, $**P \le 0.01$, and $***P \le 0.001$.

observed upregulation of the anti-inflammatory M2 marker CD206 in the alveolar macrophages. Interestingly, the Siglec-F intermediate macrophage population was not expressing either CD86 or CD206 at P8, but by P15 the upregulation of both receptors was observed (Fig. 6a and Supplementary Fig. S4a, b [online]). On the other hand, in the interstitial macrophage population, we were not able to detect either CD86 or CD206 upregulation after injury at any timepoints (Fig. 6a).

In summary, we detected a decrease in the anti-inflammatory homeostatic macrophages and an increase in a Siglec-F intermediate population of macrophages in lungs of developing 2HIT mice. However, by the age of 4 weeks, macrophage populations were similar in lungs of both RA and 2HIT animals.

Extrapulmonary manifestations in the 2HIT model

2HIT animals appeared to have transient atrophy in the spleen; mild to moderate atrophy, as well as the general structure disorganization, was observed at P14, but this was normalized by 3 months of age (data not shown). In the spleen, resident red pulp macrophages were analyzed using FACS gating strategy as described in Supplementary Fig. S2d (online) and were found to upregulate the expression of CD86 and MHCII, typical markers for M1 macrophage phenotype between P4 and P14 (Supplementary Fig. S3b [online] and Fig. 6b). Additionally, at P4–P8 we observed downregulation of CD206, indicating decrease in M2 macrophage phenotype in the spleen (Supplementary Fig. S3b [online] and Fig. 6b). However, by the age of 4 weeks the changes in spleen macrophages were reverted. No significant toxicities to the liver or the kidney were observed. In conclusion, the immune response in the 2HIT model of BPD is not limited to the lung, but involves also the spleen. No significant extrapulmonary long-term changes were observed.

DISCUSSION

The 2HIT model represents a novel platform for studying BPD pathogenesis and testing potential novel anti-inflammatory therapies. In addition, we demonstrate for the first time the innate immune response evolution in this model as a function of age, characterized by a distinct cytokine pattern and macrophage phenotype after injury.

2HIT animals showed simplified alveolar architecture and enhanced lung compliance, consistent with previous reports in murine models of BPD, as well as findings in BPD patients.[4,24] The reduced gas exchange surface area was caused by altered alveolar development characterized by decrease in secondary septation. 2HIT animals showed emphysematous functional changes, including increased compliance and an upward shift in the PV loop, reflecting decreased elastic recoil. We found no signs of long-term lung fibrosis. This to our knowledge is consistent with the current literature, as long-term fibrosis has not been reported in C57Bl/6 mouse strain after 6 days of exposure to hyperoxia.[25]

BPD patients are at higher risk of developing PH, which contributes to significant morbidity and early mortality. It has been reported that 25–35% of infants with moderate-to-severe BPD will develop PH and RVH.[26] Similarly, 2HIT mice displayed RVH at 3 months of age as measured by Fulton's index, which is most likely secondary due to PH,[27] and therefore enabling studies into PH mechanism and novel experimental therapies.

Inflammation is known to be an important risk factor for the development of BPD.[28] Epidemiological data on the role of chorioamnionitis as a risk factor for BPD are inconsistent,[29,30] but perinatal inflammation and episodes of sepsis,[14] as well as pneumonia[15] seem to be among risk factors for BPD. While other two hit models of BPD using antenatal LPS exist,[17,31,32] the current 2HIT model is novel and unique, as it combines exposure to high

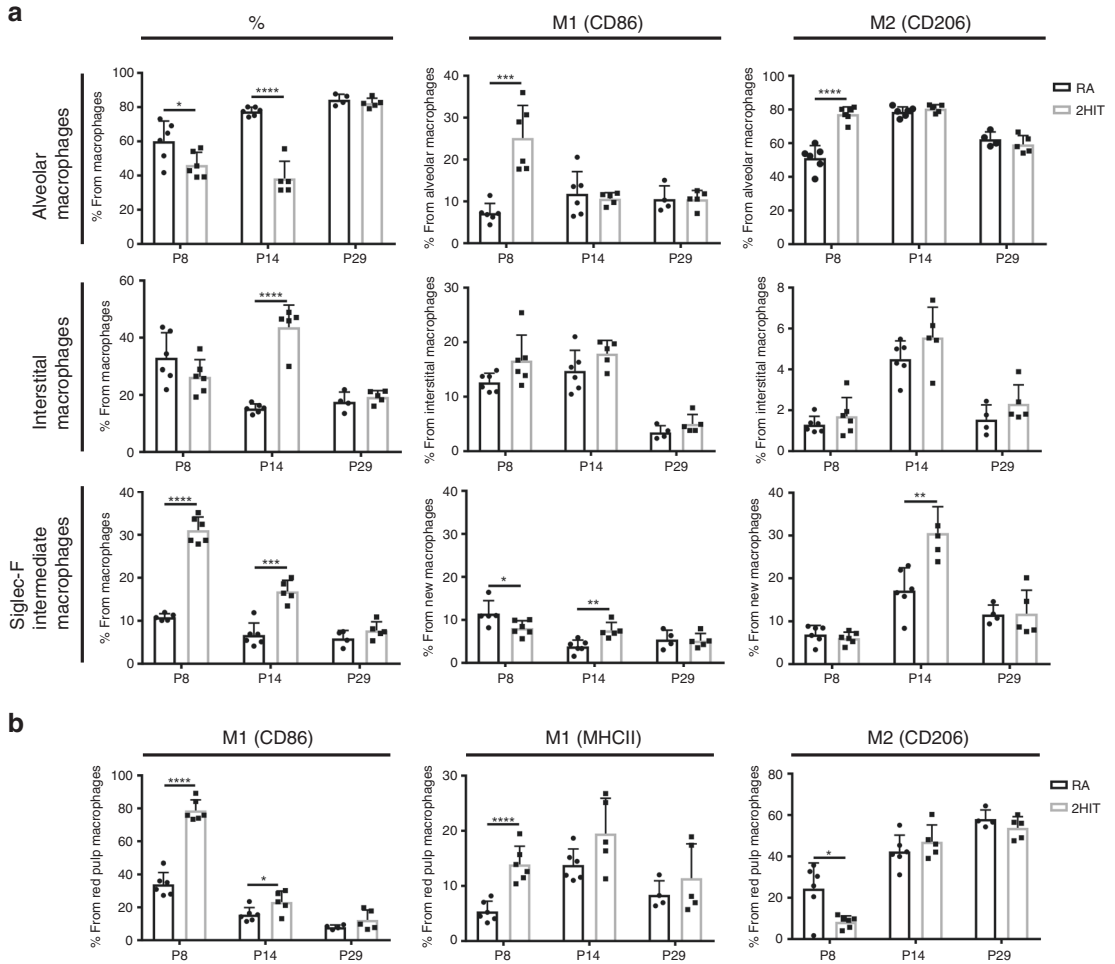

Fig. 6 Time course of lung and red pulp macrophage phenotype in the 2HIT compared to RA animals. a Lung macrophages. **b** Spleen red pulp macrophages. The values are given as relative percentages from parent populations and are represented as the means ± SD ($n = 4–6$/group). Individual data points shown for each bar graph represent individual mice from multiple litters. P value < 0.05 was considered significant. Significant results are shown as $^{*}P \le 0.05$, $^{**}P \le 0.01$, $^{***}P \le 0.001$, and $^{****}P \le 0.0001$.

level of oxygen and to postnatal inflammation. 2HIT animals demonstrated a robust inflammatory response, which in the lung is typically a cascade of events starting with activation of the coagulation and complement systems and stimulation of resident cells to promote recruitment and activation of other immune cells.[33] The hyperoxic tissue damage causes the release of intracellular proteins acting as damage associated molecular patterns. Additionally, LPS acts as a pathogen-associated molecular pattern. Both these molecular patterns are ligands to pattern recognition receptors (PRRs), such as Toll-like receptors (TLRs) on alveolar macrophages and epithelial type 2 cells, as well as on the circulating immune cells. The PRRs activated by hyperoxic injury have not been described in detail, but LPS is known to activate TLR4 through nuclear factor-κB signal transduction.[34] In our model, we show a robust initiation of inflammatory response by production of chemokines G-CSF, GM-CSF, M-CSF, KC, LIX (C-X-C motif chemokine ligand 5 [CXCL5]), MCP-1 (C-C motif chemokine ligand 2 [CCL2]), MIP-1α (CCL3), MIP-2 (CXCL2), as well as high expression of cytokines IL-1α and IL-1β, which are typically found in the initial phase of the inflammatory cascade. In the 2HIT model, the expression of IL-1β peaked in the lung at P3, indicating an early proinflammatory immune response with high levels of cytokine and chemokine expression. Interestingly, recent studies in transgenic mice have shown that early postnatal IL-1β overexpression leads to chronic lung injury similar to that seen in the hyperoxia model. This points to the important role of this cytokine in the pathogenesis of BPD.[35]

Along the increased chemokine levels, we observed recruitment of phagocytes, such as neutrophils, macrophages, and monocytes to the lungs. This correlated with a significant increase in the secretion of type 1 proinflammatory cytokines, such as IL-2, IL-6, IL-7, IL-12, IL-17, LIF, TNFα, and IFNγ. Interestingly, the gene expression levels of type 1 cytokines *Il6*, *Tnfa*, and *Tgfb1* reached a second peak in the beginning of the recovery phase one day after the pups returned to normoxia at P8. The reason for this is not yet apparent, but may indicate that the change in oxygen concentration initiates a second inflammatory response in the lungs. In addition, expression of chemokines required for the recruitment of cells of the adaptive immune system to the site of inflammation, such as RANTES (regulated upon activation, normal T cell expressed and presumably secreted) (CCL5) and MIG (CXCL9) was also upregulated.

Perturbations observed in 2HIT animals were associated with a robust change in pulmonary macrophage phenotype. We observed a decrease in alveolar macrophages and a simultaneous increase in a population of Siglec-F^{low} macrophages. The Siglec-F^{low} macrophages have previously been reported to be recruited to the lungs in an experimental fibrosis model, and lineage tracing linked the origin of these macrophages to circulating monocytes.[23] In addition to the changes in the number of macrophages,

we observed a shift from homeostatic M2 phenotype to more proinflammatory M1 phenotype in the early phases of the disease, whereas this was no longer the case at 1 month of age. This may be due to the maturation of a Siglec-F intermediate emerging macrophage population to the homeostatic phenotype. The shift in macrophage phenotype was observed in both the lung and spleen, emphasizing the fact that there is systemic involvement of the immune system in our 2HIT model. Macrophage in vivo phenotype is known to represent a spectrum of functional phenotypes rather than a simplified division to M1 and M2 categories,[36] but on the other hand, the simplified view can provide a more practical approach in terms of studying mechanism of action of novel therapies.[12]

In contrast to the increase in type 1 cytokines, we observed a significant decrease in expression of type 2 cytokines in the lungs of 2HIT animals. Type 2 cytokines are critical for resolution of inflammation and promotion of new tissue growth eventually leading to healing.[37] Transgenic mouse models have not been studied to explore the effect of type 2 cytokines in the hyperoxic lung injury of the newborn, except for IL-13, which did not protect newborn mice from hyperoxia-induced lung damage.[38] It is important to note that the type 2 response needs to be carefully balanced, as it can cause type 2 inflammation, which causes extensive pulmonary scarring and fibrosis, as well as asthma. In fact, Cheon et al.[39] reported increased expression of the type 2 cytokine genes *IL-13* and *IL-5* in the lungs of hyperoxia-exposed mice at 4 weeks of age, suggesting that hyperoxic injury results in late type 2 inflammation, which can explain the observed airway hyperreactivity. However, in our model no significant increase in type 2 cytokines was detected at 1 month of age, although we observed a trend towards increase in both the gene expression and protein levels of IL-4, IL-10, and IL-13 at this time in 2HIT animals. In fact, we detected only very early systemic type 2 cytokine production. One of the crucial functions of type 2 cytokines is to activate the adaptive immune system. The low expression level of type 2 cytokines may therefore indicate an insufficient adaptive immune response in response to the injury in the 2HIT model. However, putative changes in the adaptive immune response were beyond the scope of our study.

Our research has certain limitations. Ideally, single hit groups, RA + LPS and O_2, would be studied for all endpoints. However, neonatal LPS model has recently been characterized, and single dose of LPS was not found to cause permanent lung damage.[40] Furthermore, the neonatal hyperoxia model has been described over 30 years ago, and since then, the cytokine and immune cell changes have been characterized carefully.[7,8,11–13] Also, recently, cell atlas of single-cell transcriptome of hyperoxic neonatal lung was characterized describing the sequential (P3–P7–P14) immune cell changes in hyperoxic conditions.[41]

Our study provides the basis for unraveling the complexity of the inflammatory response in experimental BPD, which is the first and critical step in investigating the link between inflammation and impaired lung development. Future steps in this direction involve the quickly evolving field of single-cell analysis, which will represent a next level in our understanding of the molecular pathogenesis of complex diseases such as BPD on a tissue level.[10,41,42] Understanding the disease mechanism in cellular and molecular level will be essential in the clinical translation of novel therapies for BPD.

In this study, we have developed and characterized a novel 2HIT BPD model using a combination of short hyperoxia exposure (6 days) and postnatal LPS administration at P3, which more closely mimics the clinical conditions of BPD. The 2HIT model showed transient inflammation and dysplastic alveolarization with altered lung function. This model is robust and short, therefore allowing efficient preclinical testing for therapeutic interventions and exploring the disease pathogenesis, as well as mechanism of action of novel therapies.

ACKNOWLEDGEMENTS

We thank Shumei Zhong, Claudine Henoud, and Tessah Costello for technical help with RT-qPCR and MLI, Manijeh Daneshmand for expertise in pathology of extrapulmonary tissues, Chandarong Choey for expertise in flow cytometry, and Louise Pelletier Histology Core Facility of the University of Ottawa for expertise in histology. This work was supported by Canadian Institutes of Health Research (CIHR), Ontario Institute for Regenerative Medicine, the Stem Cell Network, Heart and Stroke Foundation of Canada, Finnish Sigrid Juselius Foundation, Finnish Foundation for Pediatric Research, The Canadian Lung Association, Ontario Graduate Scholarship, Molly Towel Perinatal Research Foundation, and The German Research Foundation (Deutsche Forschungsgemeinschaft).

AUTHOR CONTRIBUTIONS

C.C.-D., M.H., A.V. performed experiments; C.C.-D., M.H., I.M., F.L. analyzed data; C.C.-D., M.H. interpreted results of experiments; C.C.-D., M.H. prepared figures; C.C.-D., M.H. drafted manuscript; B.T. approved final version of manuscript; C.C.-D., M.H., A.V., I.M., F.L., B.T. edited and revised manuscript; C.C.-D., M.H., F.L., B.T. conceived and designed research.

ADDITIONAL INFORMATION

The online version of this article (https://doi.org/10.1038/s41390-020-0967-6) contains supplementary material, which is available to authorized users.

Competing interests: The authors declare no competing interests.

Publisher's note Springer Nature remains neutral with regard to jurisdictional claims in published maps and institutional affiliations.

REFERENCES

1. Johnson, T. J., Patel, A. L., Jegier, B. J., Engstrom, J. L. & Meier, P. P. Cost of morbidities in very low birth weight Infants. *J. Pediatr.* **162**, 243–249.e1 (2013).
2. Northway, W. H., Rosan, R. C. & Porter, D. Y. Pulmonary disease following respirator therapy of hyaline-membrane disease. *N. Engl. J. Med.* **276**, 357–368 (1967).
3. Jobe, A. J. The new BPD: an arrest of lung development. *Pediatr. Res.* **46**, 641–643 (1999).
4. Wong, P. M. et al. Emphysema in young adult survivors of moderate-to-severe bronchopulmonary dysplasia. *Eur. Respir. J.* **32**, 321–328 (2008).
5. Berger, J. & Bhandari, V. Animal models of bronchopulmonary dysplasia. The term mouse models. *Am. J. Physiol. Cell. Mol. Physiol.* **307**, L936–L947 (2014).
6. Nardiello, C. et al. Standardisation of oxygen exposure in the development of mouse models for bronchopulmonary dysplasia. *Dis. Model. Mech.* **10**, 185–196 (2017).
7. Bonikos, D. S., Bensch, K. G., Ludwin, S. K. & Northway, W. H. Oxygen toxicity in the newborn. The effect of prolonged 100 per cent O_2 exposure on the lungs of newborn mice. *Lab. Invest.* **32**, 619–635 (1975).
8. D'Angio, C. T., Johnston, C. J., Wright, T. W., Reed, C. K. & Finkelstein, J. N. Chemokine mRNA alterations in newborn and adult mouse lung during acute hyperoxia. *Exp. Lung Res.* **24**, 685–702 (1998).
9. Saluzzo, S. et al. First-breath-induced type 2 pathways shape the lung immune environment. *Cell Rep.* **18**, 1893–1905 (2017).
10. Cohen, M. et al. Lung single-cell signaling interaction map reveals basophil role in macrophage imprinting. *Cell* **175**, 1031–1044.e18 (2018).
11. Al-Rubaie, A. et al. The therapeutic effect of mesenchymal stem cells on pulmonary myeloid cells following neonatal hyperoxic lung injury in mice. *Respir. Res.* **19**, 114 (2018).
12. Willis, G. R. et al. Mesenchymal stromal cell exosomes ameliorate experimental bronchopulmonary dysplasia and restore lung function through macrophage immunomodulation. *Am. J. Respir. Crit. Care Med.* **197**, 104–116 (2018).
13. Johnston, C. J., Wright, T. W., Reed, C. K. & Finkelstein, J. N. Comparison of adult and newborn pulmonary cytokine mRNA expression after hyperoxia. *Exp. Lung Res.* **23**, 537–552 (1997).
14. Pryhuber, G. S. Postnatal infections and immunology affecting chronic lung disease of prematurity. *Clin. Perinatol.* **42**, 697–718 (2015).
15. Kim, H.-R. et al. Interstitial pneumonia pattern on day 7 chest radiograph predicts bronchopulmonary dysplasia in preterm infants. *BMC Pediatr.* **17**, 125 (2017).
16. Ambalavanan, N. & Morty, R. E. Searching for better animal models of BPD: a perspective. *Am. J. Physiol. Cell. Mol. Physiol.* **311**, L924–L927 (2016).
17. Tang, J.-R. et al. Moderate postnatal hyperoxia accelerates lung growth and attenuates pulmonary hypertension in infant rats after exposure to intra-amniotic endotoxin. *Am. J. Physiol. Lung Cell. Mol. Physiol.* **299**, L735–L748 (2010).

18. O'Reilly, M. A., Marr, S. H., Yee, M., McGrath-Morrow, S. A. & Lawrence, B. P. Neonatal hyperoxia enhances the inflammatory response in adult mice infected with influenza A virus. *Am. J. Respir. Crit. Care Med.* **177**, 1103–1110 (2008).
19. Hay, M., Thomas, D. W., Craighead, J. L., Economides, C. & Rosenthal, J. Clinical development success rates for investigational drugs. *Nat. Biotechnol.* **32**, 40–51 (2014).
20. Shafa, M. et al. Human induced pluripotent stem cell-derived lung progenitor and alveolar epithelial cells attenuate hyperoxia-induced lung injury. *Cytotherapy* **20**, 108–125 (2018).
21. Thébaud, B. et al. Vascular endothelial growth factor gene therapy increases survival, promotes lung angiogenesis, and prevents alveolar damage in hyperoxia-induced lung injury. *Circulation* **112**, 2477–2486 (2005).
22. Pfaffl, M. W. A new mathematical model for relative quantification in real-time RT-PCR. *Nucleic Acids Res.* **29**, e45 (2001).
23. Misharin, A. V. et al. Monocyte-derived alveolar macrophages drive lung fibrosis and persist in the lung over the life span. *J. Exp. Med.* **214**, 2387–2404 (2017).
24. Ramani, M., Bradley, W. E., Dell'Italia, L. J. & Ambalavanan, N. Early exposure to hyperoxia or hypoxia adversely impacts cardiopulmonary development. *Am. J. Respir. Cell. Mol. Biol.* **52**, 594–602 (2015).
25. Firsova, A. B., Cole, T. J. & Mollard, R. Transient vascular and long-term alveolar deficits following a hyperoxic injury to neonatal mouse lung. *BMC Pulm. Med.* **14**, 59 (2014).
26. Check, J. et al. Fetal growth restriction and pulmonary hypertension in premature infants with bronchopulmonary dysplasia. *J. Perinatol.* **33**, 553–557 (2013).
27. Shivanna, B., Reynolds, C., Zhang, S., Shrestha, A. & Barrios, R. Phenotypic assessment of pulmonary hypertension using high-resolution echocardiography is feasible in neonatal mice with experimental bronchopulmonary dysplasia and pulmonary hypertension: a step toward preventing chronic obstructive pulmonary disease. *Int. J. Chron. Obstruct. Pulmon. Dis.* **11**, 1597–1605 (2016).
28. Kallapur, S. G. Contribution of inflammation to lung injury and development. *Arch. Dis. Child. Fetal Neonatal Ed.* **91**, F132–F135 (2006).
29. Lacaze-Masmonteil, T. That chorioamnionitis is a risk factor for bronchopulmonary dysplasia—the case against. *Paediatr. Respir. Rev.* **15**, 53–55 (2014).
30. Thomas, W. & Speer, C. P. Chorioamnionitis is essential in the evolution of bronchopulmonary dysplasia—the case in favour. *Paediatr. Respir. Rev.* **15**, 49–52 (2014).
31. Nold, M. F. et al. Interleukin-1 receptor antagonist prevents murine bronchopulmonary dysplasia induced by perinatal inflammation and hyperoxia. *Proc. Natl Acad. Sci. USA* **110**, 14384–14389 (2013).
32. Choi, C. W. et al. Bronchopulmonary dysplasia in a rat model induced by intra-amniotic inflammation and postnatal hyperoxia: morphometric aspects. *Pediatr. Res.* **65**, 323–327 (2009).
33. Florez-Sampedro, L., Song, S. & Melgert, B. N. The diversity of myeloid immune cells shaping wound repair and fibrosis in the lung. *Regeneration* **5**, 3–25 (2018).
34. Lu, Y.-C., Yeh, W.-C. & Ohashi, P. S. LPS/TLR4 signal transduction pathway. *Cytokine* **42**, 145–151 (2008).
35. Hogmalm, A., Bry, M. & Bry, K. Pulmonary IL-1β expression in early life causes permanent changes in lung structure and function in adulthood. *Am. J. Physiol. Cell. Mol. Physiol.* **314**, L936–L945 (2018).
36. Arora, S., Dev, K., Agarwal, B., Das, P. & Syed, M. A. Macrophages: their role, activation and polarization in pulmonary diseases. *Immunobiology* **223**, 383–396 (2018).
37. Gieseck, R. L., Wilson, M. S. & Wynn, T. A. Type 2 immunity in tissue repair and fibrosis. *Nat. Rev. Immunol.* **18**, 62–76 (2017).
38. Choo-Wing, R., Nedrelow, J. H., Homer, R. J., Elias, J. A. & Bhandari, V. Developmental differences in the responses of IL-6 and IL-13 transgenic mice exposed to hyperoxia. *Am. J. Physiol. Cell. Mol. Physiol.* **293**, L142–L150 (2007).
39. Cheon, I. S. et al. Neonatal hyperoxia promotes asthma-like features through IL-33-dependent ILC2 responses. *J. Allergy Clin. Immunol.* **142**, 1100–1112 (2018).
40. Shrestha, A. K. et al. Consequences of early postnatal lipopolysaccharide exposure on developing lungs in mice. *Am. J. Physiol. Cell. Mol. Physiol.* **316**, L229–L244 (2019).
41. Hurskainen, K. M. et al. Multiplexed single-cell transcriptomic analysis of normal and impaired lung development in the mouse. *bioRxiv* 868802, https://doi.org/10.1101/868802 (2019).
42. Guo, M. et al. Single cell RNA analysis identifies cellular heterogeneity and adaptive responses of the lung at birth. *Nat. Commun.* **10**, 37 (2019).